Electronic Supplementary Material (ESI) for Journal of Materials Chemistry C.
This journal is © The Royal Society of Chemistry 2019

Supporting Information

Enhanced single-mode fiber laser emission by nano-crystallization of oxyfluoride glass-ceramic cores

Shiliang Kang,[a] Zhenpeng Huang,[a] Wei Lin,[a] Dandan Yang,[a] Junjie Zhao,[b] Xvsheng Qiao,[b] Xiudi Xiao,[c] Shanhui Xu,[a] Jianrong Qiu,[d] Jincheng Du[e] and Guoping Dong*[a]

[a]State Key Laboratory of Luminescent Materials and Devices, and Guangdong Provincial Key Laboratory of Fiber Laser Materials and Applied Techniques, South China University of Technology, Guangzhou 510640, China; Guangdong Engineering Technology Research and Development Center of Special Optical Fiber Materials and Devices, School of Materials Science and Engineering, South China University of Technology, Guangzhou 510640, China. E-mail: dgp@scut.edu.cn

[b]State Key Laboratory of Silicon Materials, School of Materials Science and Engineering, Zhejiang University, Hangzhou 310027, China.

[c]Key Laboratory of Renewable Energy, Guangdong Key Laboratory of New and Renewable Energy Research and Development, Guangzhou Institute of Energy Conversion, Chinese Academy of Sciences, Guangzhou 510640, China.

[d]State Key Laboratory of Modern Optical Instrumentation, College of Optical Science and Engineering, Zhejiang University, Hangzhou 310027, China.

[e]Department of Materials Science and Engineering, University of North Texas, Denton, Texas 76203-5017, U.S.

1. Thermal performance analysis of fiber samples

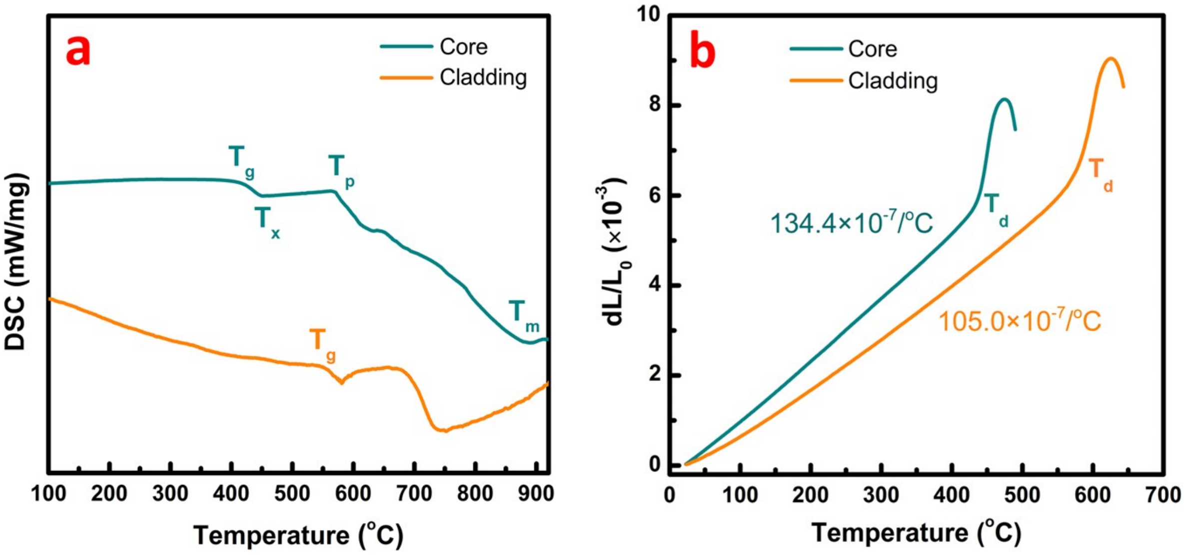

Fig. S1 Thermal properties analysis of as-prepared fiber core and cladding glass. (a) DSC curves, showing that the glass transition temperature (T_g) of fiber core and cladding glass are 421°C and 551°C, respectively. The onset crystallization temperature (T_x), crystallization peak temperature (T_p), and melting temperature (T_m) of core glass are 452°C, 562°C, and 882°C, respectively. (b) Dilatometric curves, showing that the deformation temperature (T_d) and thermal expansion coefficient of fiber core and cladding glass are 451°C, 134.4×10^{-7}/°C and 597°C, 105.0×10^{-7}/°C, respectively.

2. Absorption and transmittance spectra of as-prepared glass and GCs

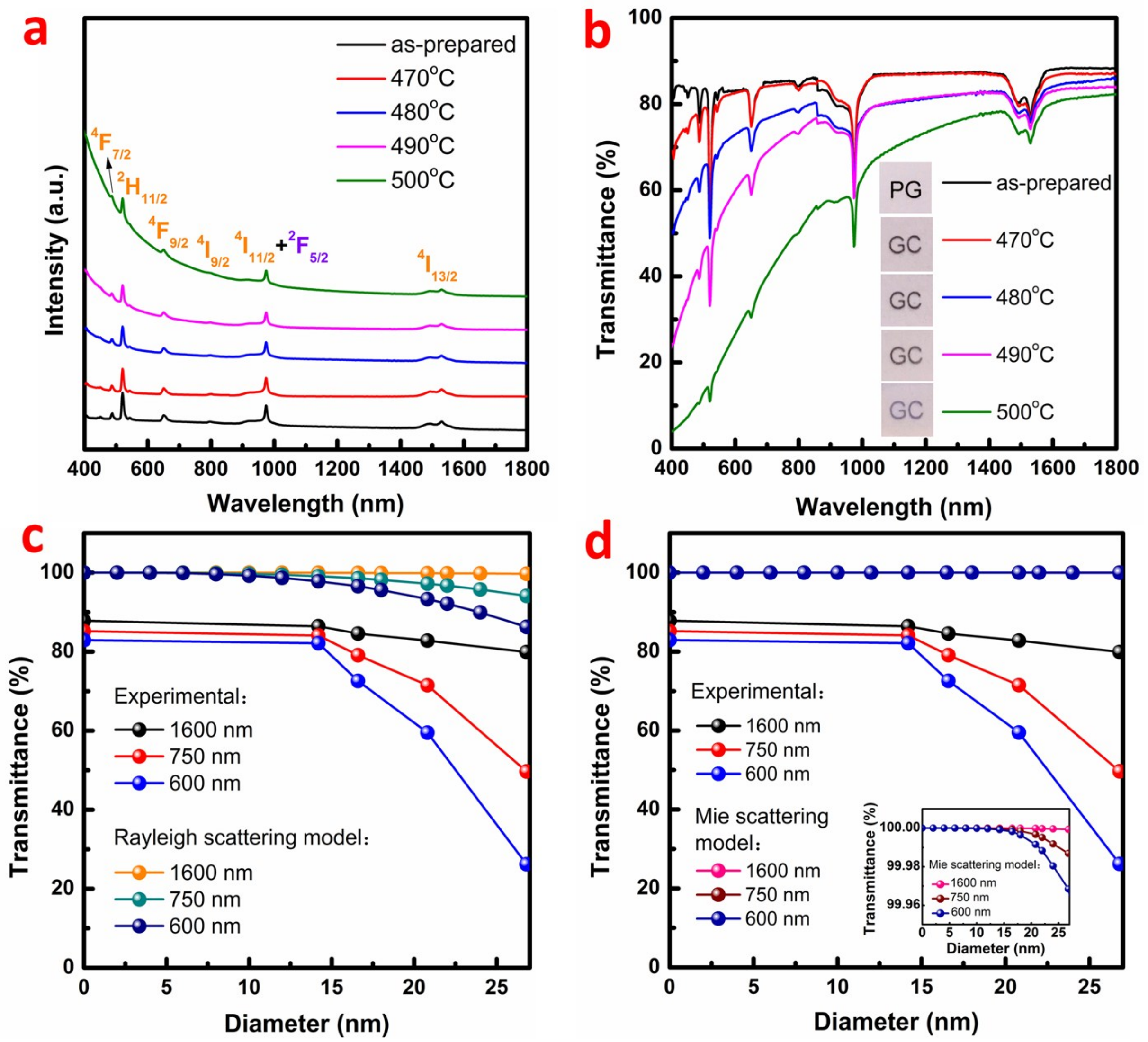

Fig. S2 (a) Absorption spectra of Er^{3+}/Yb^{3+}-codoped as-prepared glass and GCs heat-treated at different temperatures. The absorption bands centered at 1530 nm, 801 nm, 651 nm, 521 nm, and 488 nm correspond to the transitions from $^4I_{15/2}$ level to $^4I_{13/2}$, $^4I_{9/2}$, $^4F_{9/2}$, $^2H_{11/2}$ and $^4F_{7/2}$ levels of Er^{3+} ion. The enhanced absorption band centered at 976 nm is ascribed to the overlap of Er^{3+}: $^4I_{15/2}\rightarrow{}^4I_{11/2}$ and Yb^{3+}: $^2F_{7/2}\rightarrow{}^2F_{5/2}$ transitions. (b) Transmittance spectra of Er^{3+}/Yb^{3+}-codoped as-prepared glass and GCs. The transmittance of as-prepared glass is around 85%. However, the transmittance decreases sharply in the short wavelength region with the rise of heat treatment temperature, which is primarily attributed to the increased scattering loss caused by the gradual growth of nanocrystals. The inset shows the photograph of as-prepared glass with high transparency, which becomes slightly translucent with the increase of heat treatment temperature. In order to determine whether this scattering is Rayleigh scattering or Mie scattering, the transmittance of samples at 600 nm, 750 nm, and 1600 nm are calculated by using these two theoretical models.[1, 2] As can be seen from Fig. (c) and (d), the theoretical calculations from Rayleigh scattering model are more close to the experimental results, indicating that the transmittance loss is mainly caused by the Rayleigh scattering.

3. Photoluminescence properties of as-prepared glass and GCs

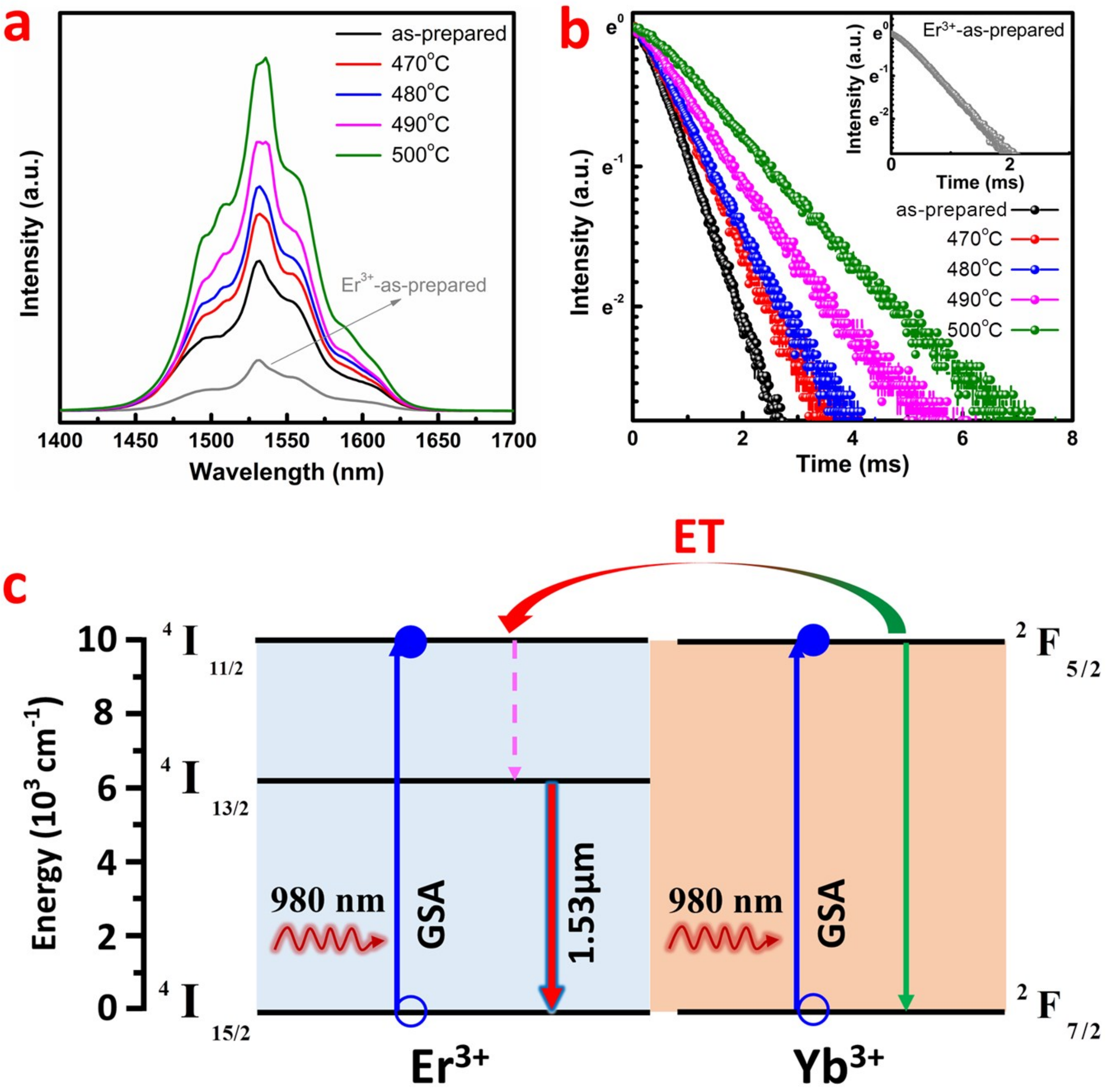

Fig. S3 (a) and (b) 1.53μm near-infrared (NIR) emission spectra and fluorescence decay curves of Er^{3+} singly and Er^{3+}/Yb^{3+}-codoped samples.

Table S1 The lifetimes of Er^{3+}:${}^4I_{13/2}$ level in Er^{3+} singly and Er^{3+}/Yb^{3+}-codoped samples

Samples	Er^{3+}	Er^{3+}/Yb^{3+}				
	as-prepared	as-prepared	470°C	480°C	490°C	500°C
τ (${}^4I_{13/2}$) (ms)	0.77	1.02	1.24	1.35	1.73	2.34

Compared to Er^{3+} singly-doped sample, the 1.53 μm NIR emission and decay lifetime obviously increase after the introduction of Yb^{3+}, which is attributed to the effective energy transfer from Yb^{3+} to Er^{3+}. With the increase of the heat treatment temperature, the NIR emission and decay lifetime monotonically increase mainly ascribed to the incorporation of Er^{3+} and Yb^{3+} into the KYF_4 nanocrystals with low phonon energy. (c) Simplified energy level diagram and energy transfer process between Er^{3+} and Yb^{3+}. Under 980 nm LD excitation, Er^{3+} ions in the $^4I_{15/2}$ level are excited to the $^4I_{11/2}$ level through ground state absorption (GSA), and meanwhile the Yb^{3+} ions in the $^2F_{7/2}$ level are pumped to the $^2F_{5/2}$ level that finally results in the population of $^4I_{11/2}$ level through the energy transfer process (ET: $^2F_{5/2}+^4I_{15/2}\rightarrow^2F_{7/2}+^4I_{11/2}$).[3] Afterwards, Er^{3+} ions excited to the $^4I_{11/2}$ level decay nonradiatively to the $^4I_{13/2}$ level and relax radiatively to the ground state by generating the 1.53 μm emission.

4. Laser performance simulation

The calculation to evaluate the laser performance is outlined as follows. Firstly, we employ the propagation equations for the pump power $P_p(z)$ and signal power $P_s^{\pm}(z)$ (± represents forward and backward propagations, respectively):[4]

$$\begin{aligned}
&\frac{\partial P_p(z)}{\partial z}=\Gamma_p\left[\sigma_{65}(\lambda_p)N_6-\sigma_{56}(\lambda_p)N_5-\sigma_{13}(\lambda_p)N_1\right]P_p(z)-\alpha P_p(z)\\
&\pm\frac{\partial P_s^{\pm}(z)}{\partial z}=\Gamma_s\left[\sigma_{21}(\lambda_s)N_2-\sigma_{12}(\lambda_s)N_1\right]P_s^{\pm}(z)\mp\alpha P_s^{\pm}(z)
\end{aligned}\tag{1}$$

The differential equations describe both the pump and signal powers in spatial coordinate z, the wavelengths of the pump and laser emission are λ_p = 980 nm and λ_s = 1550 nm, respectively. In the steady-state condition, Eq. (1) is related with the local normalized population densities n_1, n_2, n_3, and n_6 in the Er^{3+}/Yb^{3+} co-doped system, approximately described by:

$$\begin{aligned}
&W_{12}n_1-(A_{21}+W_{21})n_2+A_{32}n_3-2C_{up}N_{Er}n_2^2=0\\
&(W_{13}-A_{43})n_1-A_{43}n_2-(A_{32}+A_{43})(1-n_1-n_2)+A_{43}+C_{cr}N_{Yb}n_1n_6=0\\
&-W_{56}+(W_{65}+W_{56}+A_{65})n_6+C_{cr}N_{Er}n_1n_6=0\\
&\text{where } N_{i=1,3}=n_{i=1,3}N_{Er},\quad N_6=n_6N_{Yb}\\
&W_{12}=\frac{\Gamma_s\sigma_{12}(\lambda_s)\left(P_s^+(z)+P_s^-(z)\right)\lambda_s}{hcA_{core}},\qquad W_{21}=\frac{\Gamma_s\sigma_{21}(\lambda_s)\left(P_s^+(z)+P_s^-(z)\right)\lambda_s}{hcA_{core}}\\
&W_{13}=\frac{\Gamma_p\sigma_{13}(\lambda_p)P_p(z)\lambda_p}{hcA_{core}},\quad W_{56}=\frac{\Gamma_p\sigma_{56}(\lambda_p)P_p(z)\lambda_p}{hcA_{core}},\quad W_{65}=\frac{\Gamma_p\sigma_{65}(\lambda_p)P_p(z)\lambda_p}{hcA_{core}}
\end{aligned}\tag{2}$$

where N_{Er} and N_{Yb} are the Er^{3+} and Yb^{3+} concentration, respectively. N_i, n_i, and A_{ij} are the population density, normalized population density, and relaxation rate of the ith level, where i = 1, 2, 3, 4 indicates the $^4I_{15/2}$, $^4I_{13/2}$, $^4I_{11/2}$, $^4I_{9/2}$ levels while i = 5, 6 indicates the $^2I_{7/2}$, $^2I_{5/2}$ levels. W_{ij} is the stimulated transfer rate from i to j level, and σ_{ij} is the transition cross-section between i and j levels. C_{cr} is the cross-relaxation coefficient. Γ_p and Γ_s are the overlap factors of the pump and laser radiation. The propagation loss is denoted by α, A_{core} is the core area, $h = 6.626\times10^{-34}$ is the Planck constant and $c = 3\times10^{8}$ is the speed of light in vacuum. By imposing the following boundary conditions:

$$\begin{aligned} &P_p(0) = P_{p0} \\ &P_s^+(0) = R_1 P_s^-(0) \\ &P_s^-(L) = R_2 P_s^+(L) \end{aligned} \tag{3}$$

Eqs. (1) and (2) can be numerically solved. P_{p0} is the injected pump power, R_1 is the reflectivity of the narrow-band fiber Bragg grating, and R_2 is the reflectivity of the wide-band fiber Bragg grating. The values of the primary parameters used in the numerical calculation are as follows: $N_{\mathrm{Er}} = 1.2\times10^{26}$ m^{-3}, $N_{\mathrm{Yb}} = 1.2\times10^{26}$ m^{-3}, $A_{21} = 7.46\times10^{2}$ s^{-1}, $A_{32} = 2.8\times10^{6}$ s^{-1}, $A_{43} = 7\times10^{9}$ s^{-1}, $A_{65} = 1\times10^{3}$ s^{-1}, $\sigma_{13}(\lambda_p) = 1.68\times10^{-25}$ m^2, $\sigma_{56}(\lambda_p) = 2.357\times10^{-24}$ m^2, $\sigma_{65}(\lambda_p) = 2.938\times10^{-24}$ m^2, $\sigma_{12}(\lambda_s) = 7.46\times10^{-25}$ m^2, $\sigma_{21}(\lambda_s) = 7.85\times10^{-25}$ m^2, $C_{cr} = 2.1\times10^{-22}$ m^3/s, $\Gamma_p = \Gamma_s = 0.85$, $\alpha = 2.3$ m^{-1}, $A_{core} = 5.54\times10^{-11}$ m^2, $R_1 = 0.65$, $R_2 = 0.99$. Then the laser output is obtained by $P_{\mathrm{out}} = [1-R_1]P_s^-(0)$. Numerical results are shown in Fig. S4.

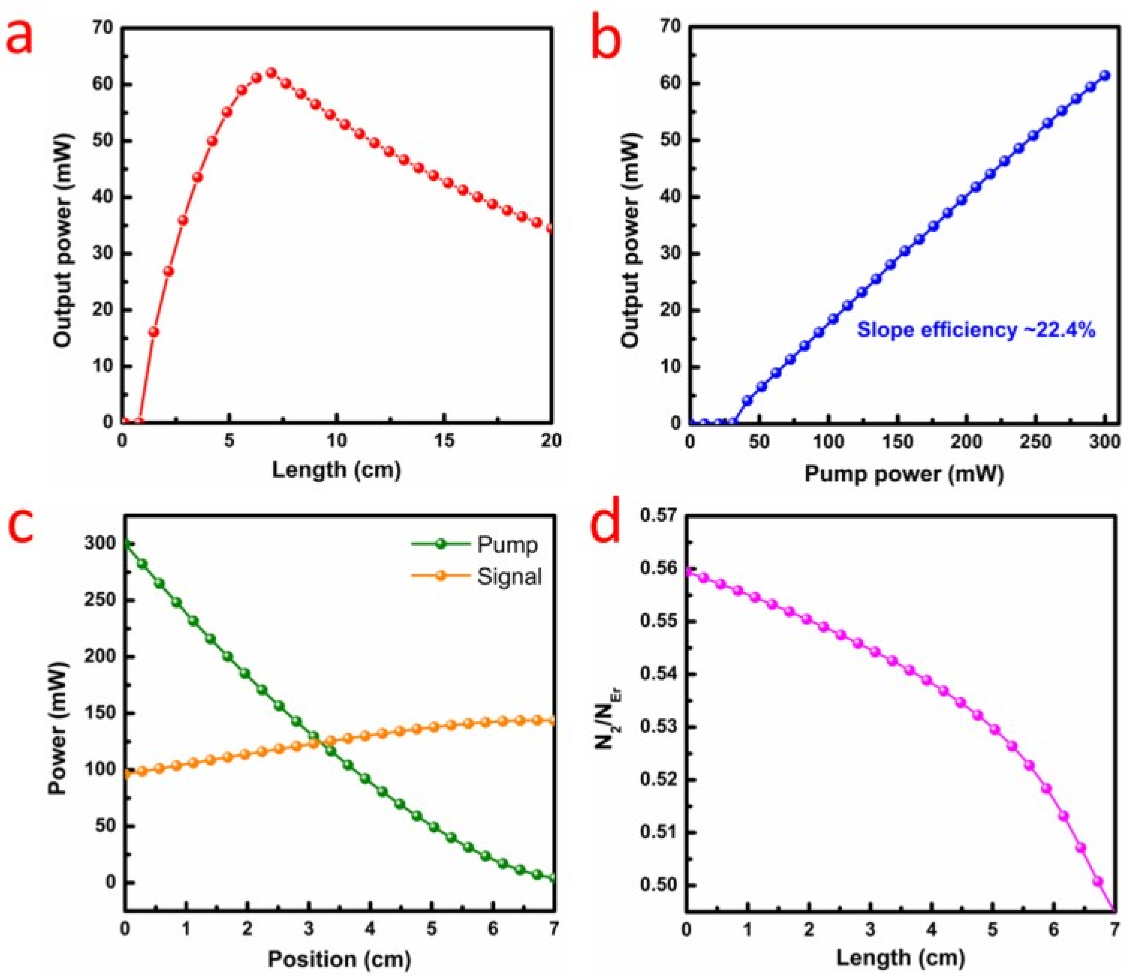

Fig. S4 (a) Output power as a function of fiber length at the pump power of 300 mW. The output power increases significantly with increasing the fiber length before reaching the maximum value, and then decreases with the further increase of fiber length. The optimum fiber length is around 7 cm. (b) Output power versus pump power for a 7-cm-long gain fiber. The output power enhances linearly with the pump power, producing a slope efficiency of 22.4% and a maximum value of 61.5 mW. (c) Pump, signal power and (d) ratio N_2/N_{Er} along a 7-cm-long gain fiber. Clearly, the signal power exhibits an increase trend with increasing the fiber length, while the pump power and the N_2/N_{Er} ratio decrease with the increase of fiber length.

References

1. Z. Wang, N. Wang, D. Wang, Z. Tang, K. Yu and W. Wei, *Opt. Lett.*, 2014, **39**, 4251.
2. J. Zhao, X. Zheng, E. P. Schartner, P. Ionescu, R. Zhang, T. Nguyen, D. Jin and H. Ebendorff-Heidepriem, *Adv. Opt. Mater.*, 2016, **4**, 1507.
3. F. T. Rabouw, P. T. Prins, P. Villanueva-Delgado, M. Castelijns, R. G. Geitenbeek and A. Meijerink, *ACS Nano*, 2018, **12**, 4812.
4. I. Kelson and A. A. Hardy, *IEEE J. Quantum. Electron.*, 1998, **34**, 1570.